



Comparison of structures and hydrophobicity of femtosecond and nanosecond laser-etched surfaces on silicon

Bao-jia Li^{a,b}, Ming Zhou^{a,b,c,*}, Wei Zhang^{a,b}, George Amoako^{a,b}, Chuan-yu Gao^b

^a School of Materials Science and Engineering, Jiangsu University, Zhenjiang 212013, PR China

^b Center for Photon Manufacturing Science and Technology, Jiangsu University, Zhenjiang 212013, PR China

^c The State Key Laboratory of Tribology, Tsinghua University, Beijing 100084, PR China

ARTICLE INFO

Article history:

Received 18 June 2012

Received in revised form 14 August 2012

Accepted 23 August 2012

Available online 2 September 2012

Keywords:

Laser

Silicon

Grating microstructures

Hydrophobicity

ABSTRACT

The rough micro- and nano- scale hierarchical structures on surfaces of materials render the surfaces superhydrophobic. In this context, we obtain both microscale grating structures and nanoscale induced structures (with some splashes) on silicon-based surfaces by means of laser etching and inducing. Our research focuses on the differences of morphology and hydrophobicity for silicon-based microstructured surfaces fabricated by femtosecond laser and nanosecond laser. The results indicated that the grating microstructures fabricated by femtosecond laser are smoother and with smaller top width of groove. Moreover, better micro-nanoscale hierarchical structures can be obtained by femtosecond laser overlapped etching for many times. On the surface with such structures, the water droplet is at Cassie–Baxter state and the contact angle (CA) is 144.6°, which indicates that the surface is middle hydrophobic. This work may provide an effective approach for fabrication of self-cleaning functional surfaces and devices.

© 2012 Elsevier B.V. All rights reserved.

1. Introduction

The hydrophobicity of solid surfaces is mainly governed by both the surface free energy and the surface roughness [1]. The hydrophobicity can be enhanced by reducing the surface free energy, but the water CA of a smooth surface even with lowest surface energy is only around 119° [2]. Thus, in order to effectively obtain a hydrophobic surface, it is necessary to create rough microstructures on the surface to make some roughness before the surface is modified by materials with low surface free energy. Since Wenzel [3] and Cassie and Baxter [4] proposed the classical wetting theories, a lot of studies have been done on the wettability of solid surfaces [5–14]. In view of the large-scale development and application of semiconductor materials, the research about wettability of silicon-based microstructured surfaces has aroused wide interest in recent years [15–21]. Laser has been applied to achieve processing, modifying and repairing on the micro- and nano- meter scale on solid surfaces because of its high machining accuracy, wide range availability of materials, short duration and high peak power. These provide a new way to fabricate silicon-based functional microstructures and microdevices. Though both femtosecond (fs) laser and nanosecond (ns) laser can be used to

fabricate silicon-based microstructures, the corresponding structure characteristics and functional features are much different from each other.

Here, we etch grating microstructures on silicon surfaces by fs laser and ns laser respectively. The effect of silicon-based microstructures on wettability is discussed and the morphology characteristics and hydrophobicity of silicon-based surfaces are comparatively analyzed.

2. Experimental

2.1. Samples fabrication

In our experiment, we used n-type silicon (100) square plates with side length of 10 mm. The samples were soaked in 5% (mass fraction) hydrofluoric acid for 15 min, and were cleaned with 10 min ultrasonic baths in deionized water, anhydrous ethanol and acetone respectively, followed by blowing nitrogen over to dry the surfaces.

Both Integra-C-2.5-SHG fs laser system (Quantronix Inc., USA) which can provide a laser beam with central wave length of 800 nm, pulse width of 130 fs, frequency of 1 kHz and max single pulse energy of 1 mJ; and Wedge532 ns laser system (Bright Solution Ltd., Italy) which can provide a laser beam with central wave length of 532 nm, pulse width of 1–2 ns, frequency of 1 kHz and max single pulse energy of 0.9 mJ, were used for the experiment. The fs and ns laser beams were both of Gaussian intensity distributions and

* Corresponding author at: School of Materials Science and Engineering, Jiangsu University, Zhenjiang 212013, PR China. Tel.: +86 511 88791458; fax: +86 511 88791288.

E-mail address: zm.laser@126.com (M. Zhou).

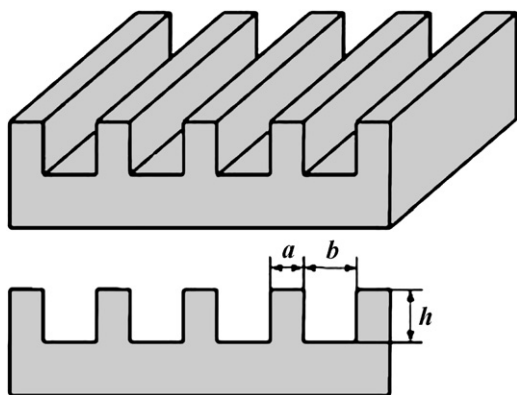


Fig. 1. A model of the grating microstructure on silicon surface.

vertically irradiated on the surfaces of samples after being focused to a diameter of $\sim 90\ \mu\text{m}$ by long focal lenses. During the fabrication, the positions of both laser beams were controlled by the movement of the dual galvanometer commanded by a computer.

A model of the grating microstructure on silicon surface used for laser etching is shown in Fig. 1. The geometric parameters of grating microstructures were designed as $90\ \mu\text{m}$ for the top width of the gratings (a), $40\ \mu\text{m}$ for the depth of the grooves (h), $90\ \mu\text{m}$, $110\ \mu\text{m}$, $130\ \mu\text{m}$ and $150\ \mu\text{m}$ for the top widths of the grooves (b). Two groups of samples named F (by fs laser) and N (by ns laser) were fabricated by scanning 10 times through the laser beam with a velocity of $1\ \text{mm/s}$. Each group included four samples which were numbered as 1, 2, 3 and 4 in accordance with the order of the top widths of the grooves b from small to large. To obtain the pre-designed depth of the grooves h and take into consideration the fact that the light absorption of silicon at $800\ \text{nm}$ is lower than that at $532\ \text{nm}$ [22], the fs laser fluence and ns laser fluence were selected as $5.1\ \text{J/cm}^2$ and $3.2\ \text{J/cm}^2$ respectively.

2.2. Samples after treatment

After etching with laser, the samples were cleaned with a 10 min ultrasonic bath in deionized water, followed by blowing nitrogen over to dry the surfaces. Then the samples were silanized in a

vacuum oven ($90\ ^\circ\text{C}$, $0.1\ \text{Torr}$) for 4 h using silane reagent (Trichloro (1H, 1H, 2H, 2H-perfluorooctyl) silane, 97%) to lower their surface energy.

2.3. Samples characterization

The samples were examined by JSM-2800LV scanning electron microscopy (SEM) (JEOL Ltd., Japan). Water CAs on the surfaces of samples were measured by OCA20 video optic CA instrument (Dataphysics Co., Germany) and the selected water droplet volume was $V = 1\ \mu\text{L}$. The water CA on each sample surface was measured for five times and the average value named as θ' was adopted.

3. Results and discussion

3.1. Comparison of morphology

Fig. 1 shows the SEM images of grating microstructures on sample surfaces fabricated by fs and ns lasers. A uniform distribution of gratings and grooves is observed for each surface. Some micro-scale holes form at the bottom of the grooves etched by fs laser (Fig. 2(a) and (b)), which is probably due to the selected larger laser fluence. There are few splashes deposited on the edges of the gratings with very small covered scopes and the outlines of edges are slightly smooth (Fig. 2(c)). There is almost no induced hole appearing at the bottom of the grooves etched by ns laser (Fig. 2(d) and (e)). There are also splashes on the edges of the gratings, and it can be seen from Fig. 2(f) that the splashes are many and cover larger scopes so that the surface roughness has to some extent increased. Furthermore, Fig. 2(c) and the inset in Fig. 2(f) show that the grooves etched by fs and ns lasers are both V-shaped, which relevant to the Gaussian intensity distribution of fs and ns laser beams.

By observing the morphologies on the surfaces of all the silicon-based samples, it is found that the top width of the gratings a are stable in each group. But the value a for each sample in group F is all slightly bigger than that in group N, which is probably due to the very small heat-affected zone for fs laser irradiating silicon surfaces compared with the large heat-affected zone, obvious ablated trace and massive splashes caused by dominant heat effect for ns laser irradiating silicon surfaces [23]. The comparison of designed value and actual values for the top widths of the grooves b on each sample

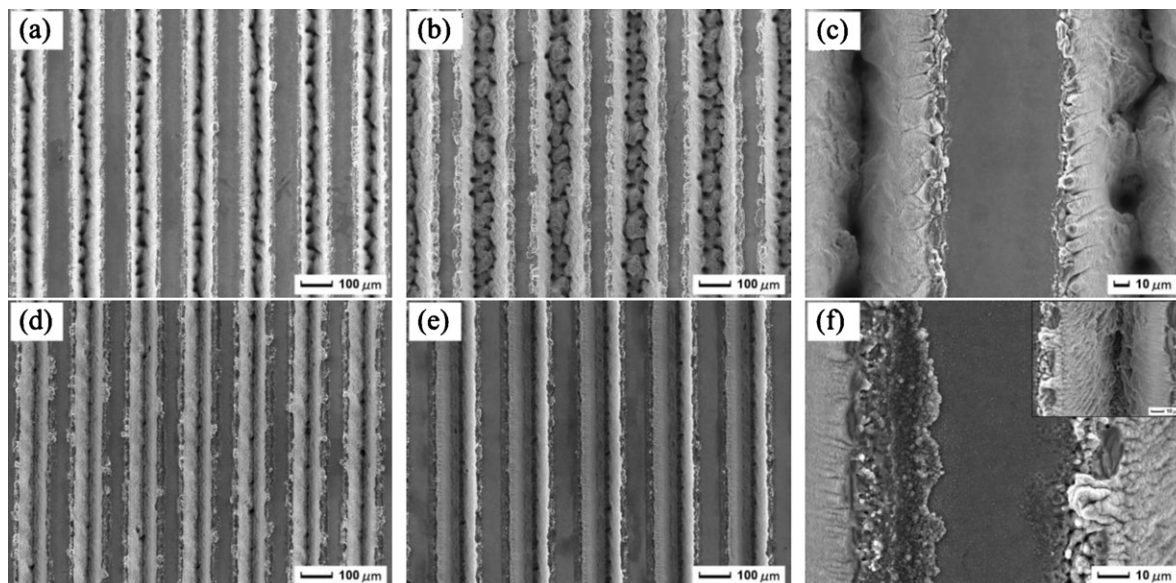


Fig. 2. SEM images of the grating microstructures on laser-etched surfaces. (a) $b = 90\ \mu\text{m}$, by fs laser. (b) $b = 150\ \mu\text{m}$, by fs laser. (c) An enlarged view for top side of the grating in (a). (d) $b = 90\ \mu\text{m}$, by ns laser. (e) $b = 150\ \mu\text{m}$, by ns laser. (f) An enlarged view for top side of the grating in (d), the inset is an enlarged view for the groove in (d).

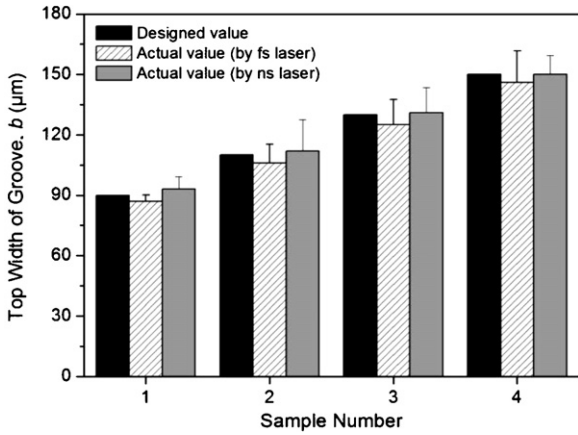


Fig. 3. Comparison of designed value and two actual values (by fs laser and ns laser) for the top widths of the grooves *b* on each of the four sample surfaces.

surface shown in Fig. 3 also illustrates this point. It can be seen from Fig. 3 that the values of *b* obtained by fs laser etching are all smaller than the corresponding designed values while the ones obtained by ns laser etching are all larger than the corresponding designed values. The zone of laser effect is greatly reduced by the “cold” processing of fs laser, but the edge of laser-affected zone is ablated and damaged to a certain extent by a strong heat effect of ns laser, which may contribute to the comparison result in Fig. 3.

The depths of the grooves are obtained by laser scanning 10 times. Compared with the method of scanning once with larger laser fluence, scanning many times can greatly reduce splashes and improve surface quality. Fig. 4 shows side-view optical images of the grating microstructures. There are no significant differences in overall depths of the grooves which are nearly the same as the designed values (*h* = 40 µm). As mentioned, ns laser etching causes obvious ablated trace and relatively massive splashes, so the appearance of the grating structure etched by ns laser (Fig. 4(b)) is more blur than that etched by fs laser (Fig. 4(a)).

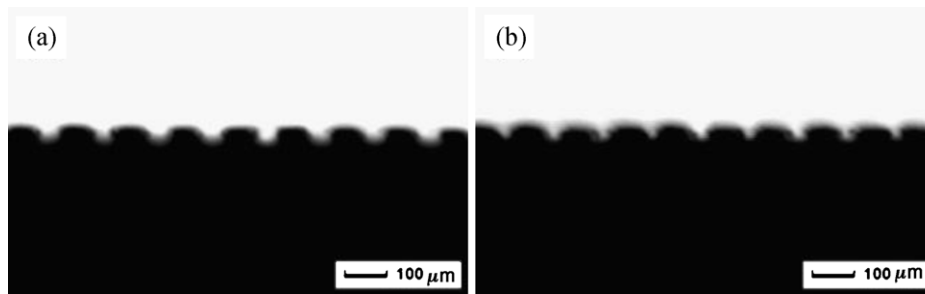


Fig. 4. Side-view optical images of the grating microstructures etched by fs laser (a) and ns laser (b).

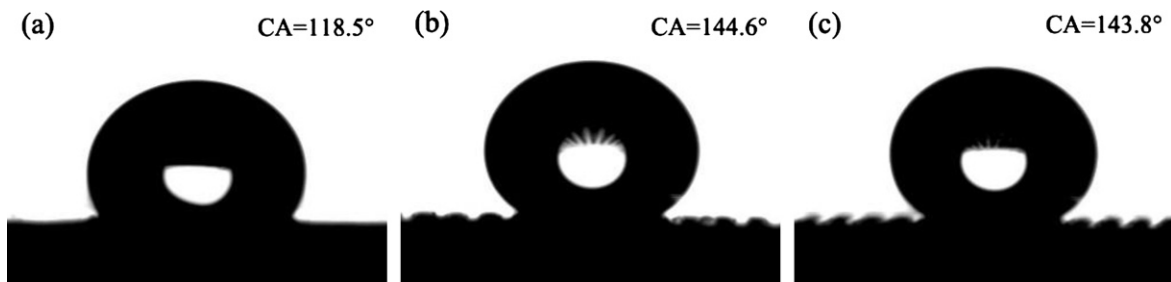


Fig. 5. Photographs of water droplets on flat (a), fs laser etched (b) and ns laser etched (c) silicon-based surfaces after silanization.

3.2. Wettability of grating microstructured surface

As a hydrophilic surface, silicon surface will become hydrophobic by either coating materials with low surface free energy or creating rough microstructures on the surface, and the effect of the coatings can be significantly enhanced by the surface roughness [20]. In order to investigate the effect of microstructure on wettability of silicon surface, the grating microstructure on silicon surface etched by laser is idealized as the model shown in Fig. 1. Therefore the Wenzel and Cassie–Baxter equations [3,4] can be expressed by

$$\cos \theta_r^W = \left[1 + \frac{2h}{a+b} \right] \cos \theta_e \tag{1}$$

$$\cos \theta_r^{CB} = -1 + \frac{a}{a+b} (\cos \theta_e + 1) \tag{2}$$

Here, θ_r^W , θ_r^{CB} and θ_e are the contact angles for Wenzel state, Cassie–Baxter state and a flat solid surface, respectively; *a*, *b* and *h* are the top width of the gratings, the top widths and the depth of the grooves, respectively. It can be inferred from Eqs. (1) and (2) that θ_r^W will be smaller than θ_e , and θ_r^{CB} will be larger than θ_e if $\theta_e < 90^\circ$, θ_r^W and θ_r^{CB} will both increase with increasing *b*; instead, θ_r^W and θ_r^{CB} will both be larger than θ_e if $\theta_e > 90^\circ$, θ_r^W will reduce and θ_r^{CB} will increase with increasing *b*.

Wettability of the silicon-based surfaces is distinguished through CA. Samples microstructured by laser and flat samples are all silanized to lower the surface energy. Fig. 5 shows photographs of water droplets on flat, fs laser etched and ns laser etched silicon-based surfaces. The CA on the flat surface is 118.5° as shown in Fig. 5(a). The values of θ_r^W and θ_r^{CB} calculated by Eqs. (1) and (2) are listed in Table 1 with the measured values θ' . It is found from Table 1 that hydrophobicity on all microstructured silicon-based surfaces is enhanced to a certain extent. In other words, the low hydrophobic flat silicon-based surface becomes middle hydrophobic after being etched with grating structures by fs or ns laser. The maximum measured CA on surfaces microstructured by fs laser is up to 144.6° (Fig. 5(b)), which has relative deviations of 11.66% and 0.77% from calculated θ_r^W and θ_r^{CB} respectively. While the maximum measured CA on surfaces microstructured by ns laser is 143.8° (Fig. 5(c)), which has relative deviations of 11.04% and 0.21% from calculated

Table 1
Measured and calculated results of CAs on the surfaces of the silicon-based samples in two groups.

Sample number	h (μm)	a (μm)	b (μm)	θ_r^W ($^\circ$)	θ_r^{CB} ($^\circ$)	θ' ($^\circ$)	
						Group F	Group N
1	40	90	90	133.6	137.6	136.8	139.8
2			110	131.9	139.9	139.2	141.8
3			130	130.6	141.8	142.7	142.0
4			150	129.5	143.5	144.6	143.8

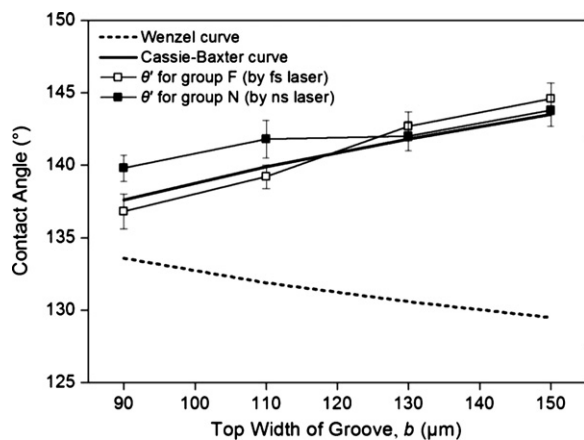


Fig. 6. Contrasting curves of measured CA (θ') and calculated CAs (θ_r^W and θ_r^{CB}) for the four sample surfaces in each group.

θ_r^W and θ_r^{CB} respectively. Consequently, it can be affirmed that the water droplets form Cassie–Baxter states on the microstructured silicon-based surfaces. Furthermore, as showed in Table 1, the measured CA on the sample surfaces in both group F and group N shows increasing trend with the increase in b , which also agrees with the Cassie–Baxter state described by Eq. (2). This proves that hydrophobicity on a silicon-based surface can be controlled by laser microstructuring with different parameters.

3.3. Comparison of hydrophobicity

Fig. 6 shows contrasting curves of measured and calculated CAs for the four sample surfaces in each group as listed in Table 1. It is obvious that for the samples in both group F and group N, the agreement of the measured CAs (θ') with the calculated CAs (θ_r^{CB}) that have not taken the effect of nanostructures on the gratings into account is good provided. This result further proves that the water droplets are all at Cassie–Baxter states on the surfaces of the samples in the two groups.

As mentioned above, the actual values of b obtained by fs laser etching are all smaller and the ones obtained by ns laser etching are all larger than the corresponding designed values, while θ_r^{CB} will increase with the increase in b for $\theta_e > 90^\circ$ by analyzing Eq. (2). Thus it is clear that when other conditions are the same, the measured CAs for samples microstructured by ns laser should be a little larger than the calculated θ_r^{CB} , while the measured CAs for samples microstructured by fs laser should be a little smaller than the calculated θ_r^{CB} . The former agrees with the corresponding result showed in Fig. 6, but the latter is rather different. Fig. 6 shows that for the samples microstructured by fs laser, θ' for larger values of b are slightly larger than θ_r^{CB} and even larger than that for the samples microstructured by ns laser, which is maybe related to the morphology characteristics of sample surfaces.

In order to explain reasons for the subtle differences above, the effects of nanoscale structures on the gratings are analyzed below by some enlarged views of the grating structures shown in Fig. 7. In our experiment, the laser scan paths are staggered and overlapped many times to obtain the larger values of b ,

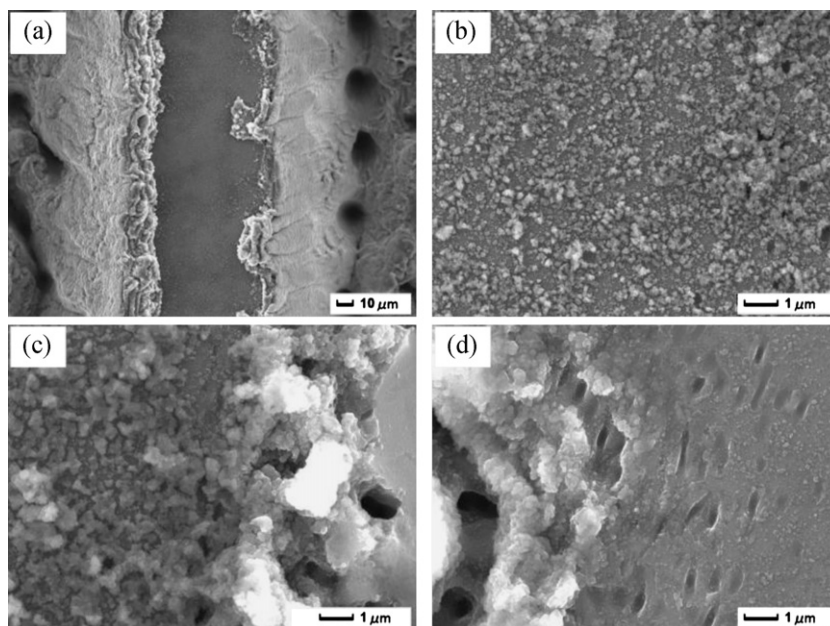


Fig. 7. SEM images of the local morphologies for grating microstructures on laser-etched surfaces. (a) An enlarged view of top side of the grating in Fig. 1(b). (b) A local enlarged view for top side center of the grating in (a). (c) A local enlarged view for top side edge of the grating in (a). (d) A local enlarged view for top side edge of the grating in Fig. 1(e).

meanwhile the selected laser fluence for fs laser etching is relatively large (5.1 J/cm^2). All these result in formation of a nanostructure layer composed of more splashes and induced structures on the micro-scale grating structure (Fig. 7(a)–(c)). This micro-nanoscale hierarchical structure can enhance the hydrophobicity of sample surfaces [24], thus the θ' as an evaluation index for hydrophobicity has a certain degree of increase. But when it comes to the sample surfaces etched by ns laser, the generated massive splashes and induced structures can be incessantly fused and eliminated by intense heat effect accumulated during laser overlapped scanning. Therefore only few microprotuberance structures formed by solidification of the fusants remain at the edge of the laser-affected zone (Fig. 7(d)), which contributes less to the increase in θ' on the sample surfaces.

4. Conclusion

In conclusion, we have contrastively investigated the morphology characteristics and hydrophobicity of silicon-based surfaces with grating microstructures fabricated by fs and ns lasers. Some even-distributed and regular-shaped grating structures can be etched by both fs and ns lasers on silicon-based surfaces, but the fs laser etched structures are relatively smooth with fewer splashes and smaller top widths of grooves. The silicon-based surfaces all have a significant enhancement in hydrophobicity after being microstructured by both fs and ns lasers. While in the case of overlapped scanning for many times, fs laser etching on silicon-based surfaces results in preferable micro-nanoscale hierarchical structures, which contribute a lot to the enhancement of hydrophobicity on the surfaces. Compared with a grating microstructured surface, a surface with square pillar microstructures [8] or other morphologies abstractly has better hydrophobicity, so a surface with composited nanostructures on square pillar microstructures or other morphologies by fs laser etching is expected to achieve superhydrophobicity. Obviously, this work provides a basis and reference for fabrication of silicon-based superhydrophobic surfaces.

Acknowledgments

This work is supported by Jiangsu Province Research Innovation Program of College Graduate (grant no. CX08B.053Z), a project funded by the Priority Academic Program Development of Jiangsu Higher Education Institutions, National Key Basic Research Development Program of China (973 Program, grant no. 2011CB013004) and the National Natural Science Foundations of China (grant no. 50975129 and 50975128).

References

- [1] L. Feng, S.H. Li, Y.S. Li, H.J. Li, L.G. Zhang, J. Zhai, Y.L. Song, B.Q. Liu, L. Jiang, D.B. Zhu, Super-hydrophobic surfaces: from natural to artificial, *Advanced Materials* 14 (2002) 1857–1860.
- [2] T. Nishino, M. Meguro, K. Nakamae, M. Matsushita, Y. Ueda, The lowest surface free energy based on $-\text{CF}_3$ alignment, *Langmuir* 15 (1999) 4321–4323.
- [3] R.N. Wenzel, Resistance of solid surfaces to wetting by water, *Industrial and Engineering Chemistry* 28 (1936) 988–994.
- [4] A.B.D. Cassie, S. Baxter, Wettability of porous surfaces, *Transactions of the Faraday Society* 40 (1944) 546–551.
- [5] C. Peigen, X. Ke, O.V. Joseph, R.H. James, The microscopic structure of adsorbed water on hydrophobic surfaces under ambient conditions, *Nano Letters* 11 (2011) 5581–5586.
- [6] J.B. Lee, H.R. Gwon, S.H. Lee, M. Cho, Wetting transition characteristics on microstructured hydrophobic surfaces, *Materials Transactions* 51 (2010) 1709–1711.
- [7] M.J.D. Anthony, L. Eric, The friction of a mesh-like super-hydrophobic surface, *Physics of Fluids* 21 (2009) 113101.
- [8] B.J. Li, M. Zhou, R. Yuan, L. Cai, Fabrication of titanium-based microstructured surfaces and study on their superhydrophobic stability, *Journal of Materials Research* 23 (2008) 2491–2499.
- [9] M. Nosonovsky, Multiscale roughness and stability of superhydrophobic biomimetic interfaces, *Langmuir* 23 (2007) 3157–3161.
- [10] L. Biao, F.L. Fred, Pressure induced transition between superhydrophobic states: Configuration diagrams and effect of surface feature size, *Journal of Colloid and Interface Science* 298 (2006) 899–909.
- [11] B. Krasovitski, A. Marmur, Drops down the hill: theoretical study of limiting contact angles and the hysteresis range on a tilted plate, *Langmuir* 21 (2005) 3881–3885.
- [12] T.N. Krupenkin, J.A. Taylor, T.M. Schneider, S. Yang, From rolling ball to complete wetting: the dynamic tuning of liquids on nanostructured surfaces, *Langmuir* 20 (2004) 3824–3827.
- [13] B. He, N.A. Patankar, J. Lee, Multiple equilibrium droplet shapes and design criterion for rough hydrophobic surfaces, *Langmuir* 19 (2003) 4999–5003.
- [14] L. Feng, S.H. Li, H.J. Li, J. Zhai, Y.L. Song, L. Jiang, D.B. Zhu, Super-hydrophobic surface of aligned polyacrylonitrile nanofibers, *Angewandte Chemie International Edition* 41 (2002) 1221–1223.
- [15] B. Nunes, A.P. Serro, V. Oliveira, M.F. Montemor, E. Alves, B. Saramago, R. Colaço, Ageing effects on the wettability behavior of laser textured silicon, *Applied Surface Science* 257 (2011) 2604–2609.
- [16] C.D. Gu, J.P. Tu, T.Y. Zhang, Deposition and wettability of silver nanostructures on Si(1 0 0) substrate based on galvanic displacement reactions, *Applied Surface Science* 257 (2010) 1779–1785.
- [17] X.C. Li, B.K. Tay, P. Miele, A. Brioude, D. Cornu, Fabrication of silicon pyramid/nanowire binary structure with superhydrophobicity, *Applied Surface Science* 255 (2009) 7147–7152.
- [18] Y.H. Liu, X.K. Wang, J.B. Luo, X.C. Lu, Fabrication and tribological properties of super-hydrophobic surfaces based on porous silicon, *Applied Surface Science* 255 (2009) 9430–9438.
- [19] A. Winkleman, G. Gotesman, A. Yoffe, R. Naaman, Immobilizing a drop of water: fabricating highly hydrophobic surfaces that pin water droplets, *Nano Letters* 8 (2008) 1241–1245.
- [20] B.J. Li, M. Zhou, K.X. Qian, L. Cai, Design and fabrication of super-hydrophobic surfaces on silicon wafers and study of effects to hydrophobicity, *Chinese Journal of Mechanical Engineering* 21 (2008) 18–21.
- [21] X.Y. Song, J. Zhai, Y.L. Wang, L. Jiang, Self-assembly of amino-functionalized monolayers on silicon surfaces and preparation of superhydrophobic surfaces based on alkanolic acid dual layers and surface roughening, *Journal of Colloid and Interface Science* 298 (2006) 267–273.
- [22] C.H. Crouch, J.E. Carey, M.Y. Shen, E. Mazur, F.Y. Génin, Infrared absorption by sulfur-doped silicon formed by femtosecond laser irradiation, *Applied Physics A* 79 (2004) 1635–1641.
- [23] B.N. Chichkov, C. Momma, S. Nolte, F. von Alvensleben, A. Tünnermann, Femtosecond, picosecond and nanosecond laser ablation of solids, *Applied Physics A* 63 (1996) 109–115.
- [24] N.A. Patankar, Mimicking the lotus effect: influence of double roughness structures and slender pillars, *Langmuir* 20 (2004) 8209–8213.